

Article

Pore Structure Characteristics and Main Control Factors of Sandstone in the Jurassic Zhiluo Formation in the Northern Ordos Basin

Xiaofeng Liu ¹, Xiaodan Guo ^{2,3}, Zenglin Hong ^{1,2,*}, Xuping Xue ² and Shifeng Li ¹

¹ School of Land Engineering, Chang'an University, Xi'an 710054, China; 2019027017@chd.edu.cn (X.L.); 2020035004@chd.edu.cn (S.L.)

² Shaanxi Institute of Geological Survey, Xi'an 710054, China; lxgeo@163.com (X.G.)

³ Shaanxi Provincial Mineral Geological Survey Center, Xi'an 710000, China

* Correspondence: lhqhzl@163.com; Tel.: +86-29-8965-0391

Abstract: The Jurassic Yan'an Formation in the Ordos Basin is one of the main coal seams mined in the basin, and the enrichment of water bodies in the upper part of this coal seam is closely related to the sand bodies in the Zhiluo Formation. This study is based on the use of core observations in the northern part of the Ordos Basin for studying the pore characteristics of the permeable sand layer of the Zhiluo Formation in the study area through testing methods such as ordinary thin sections, cast thin sections, scanning electron microscopy (SEM), mercury intrusions, and physical property analysis. The results indicate that the primary pores of the Zhiluo Formation sandstone in the study area include primary intergranular pores, residual intergranular pores, and interstitial micropores. The secondary pores are mainly intergranular pores, feldspar dissolution pores, and rock debris dissolution pores. The throat-type pores are mainly variable fault contractions, sheets, curved sheets, and bundle-shaped throats. The pore structures of the Zhiluo Formation sandstone in the research area are complex, and the permeability is influenced by the throat characteristics. The main controlling factors of the pore structure characteristics of the Zhiluo Formation sandstone in the study area are sedimentation and diagenesis. Compaction and cementation are the main factors that destroy the sandstone pore structure, while later dissolution plays a certain role in the improvement of the pores. Section 1 of the Zhiluo Formation is greatly affected by diagenesis, and section 2 is greatly affected by sedimentation.

Keywords: pore structure; main control factors; Zhiluo Formation; Ordos Basin



Citation: Liu, X.; Guo, X.; Hong, Z.; Xue, X.; Li, S. Pore Structure Characteristics and Main Control Factors of Sandstone in the Jurassic Zhiluo Formation in the Northern Ordos Basin. *Minerals* **2023**, *13*, 1102. <https://doi.org/10.3390/min13081102>

Academic Editor: Thomas Gentzis

Received: 3 June 2023

Revised: 11 August 2023

Accepted: 16 August 2023

Published: 18 August 2023



Copyright: © 2023 by the authors. Licensee MDPI, Basel, Switzerland. This article is an open access article distributed under the terms and conditions of the Creative Commons Attribution (CC BY) license (<https://creativecommons.org/licenses/by/4.0/>).

1. Introduction

The pore structure is a key factor in tight sandstone reservoirs and restricts the accumulation and flow of oil and gas in such reservoirs. The pore structure of reservoirs has been a focus and challenges faced in recent unconventional oil and gas exploration and development research. With the increasing demand for oil and natural gas, the difficulty of exploration and development has also increased. Global oil and gas exploration and development have shifted from conventional oil and gas sources to unconventional sources such as shale oil, tight oil, and coal bed methane (CBM) [1–3].

At present, the research methods applied to determine pore structure characteristics can be divided into two categories: mathematical statistics analysis methods and computer simulation methods [4,5]. Among the mathematical statistics analysis methods, conventional mercury injections reflect the pore characteristics under a semiquantitative static state [6–8]. Constant velocity mercury injections are effective for pore sizes greater than 0.12 µm in quantitative research on pores and throats [9]. High-pressure mercury intrusions are used mainly for the determination of dense rocks [7]. Rezaee [10] and Zheng et al. [11]

introduced nuclear magnetic resonance into a pore characteristic study in complex lithologic reservoirs, but the method could not truly reflect the complex underground pore structure characteristics [12,13]. Elliot [14] and Yoshito [15] applied CT scanning to perform a three-dimensional reconstruction of pores and established a microscopic seepage model. Low-temperature adsorption is mainly used in research on shale and coal rocks [16,17]. Among the computer simulation methods, digital core technology can achieve the three-dimensional model reconstruction of internal rock pores [18–20]. Yao et al. [21], Zhao et al. [22], Zhu et al. [23], and Zhu [24] carried out simulation research on the single-phase fluid in the seepage process. From the methods used to describe the fractal geometry of rock cores, reservoir pores are thought to have good fractal structural properties that are not affected by the scale and can form a bridge between the micropore structure and macroscopic rock physical parameters [25–27].

In the pore evolution process, the impact factors include compaction, the shale mineral composition, the vitrinite reflectance (R_o , %), and the organic matter abundance and type [28]. Previous studies on the influencing factors of shale pore development have been extensive, and it is generally believed that the abundance, type, and maturity of organic matter, as well as the composition of rock minerals, significantly impact shale pore development [28,29]. Most researchers noted that the R_o and total organic carbon (TOC, %) contents are important factors affecting the development of shale pores [30–32]. Some scholars have reported that the clay mineral content in mineral components can also affect the pore volume and specific surface area of shale to a certain extent [30]. The main controlling factors of sandstone pore structure have been studied by scholars. Wu et al. [33] believe that diagenesis is the main factor controlling the pore structure of Shahejie Formation sandstone in the Bohaiwan Basin, Wang et al. [34] believe that lithology and diagenetic fluid jointly control the development of secondary pores in Benxi Formation sandstone, and Feng et al. [35] believe that compaction is the main factor controlling the pore structure of sandstone reservoir.

In a study on the sandstone pore structure in the Ordos Basin, the Yanchang Formation was found to be relatively mature, and scholars have systematically studied the pore structure characteristics of the sandstone in different layers of the Yanchang Formation [36–40]. With the increasing demand for oil and the increasing difficulty of oil extraction, researchers have noted the low permeability pores of the Yanchang Formation [41–43]. Compared to the highly researched Yanchang Formation, research studies on the pore structure of sandstones in the Zhiluo Formation in the northeastern Ordos Basin are relatively lacking.

2. Geological Setting

The Ordos Basin is located in the North China Craton. In the western part, a multitectonic system containing multiple sedimentary types, depression migration, and significantly distorted multicycle superimposed oil- and gas-bearing basins have developed [39,40]. The research area is located on the Yimeng Uplift in the northern part of the Ordos Basin and has been one of the main areas for analyzing sandstone-type uranium deposits in recent years (Figure 1). The terrain is characterized by steep slopes in the northwest and shallow slopes in the southeast [44].

The Zhiluo Formation in the Ordos Basin generally has two distinct sedimentary cycles, and Zhao et al. [45] divided the Zhiluo Formation into upper and lower segments. Section 1 of the Zhiluo Formation contains mainly braided river deposits, while section 2 of the Zhiluo Formation contains meandering river deposits [46]. The lower part of section 1 of the Zhiluo Formation is a set of extremely thick, chertreuse, moderately coarse arkose and lithic arkose. Cross-bedding is developed in this section and is generally characterized by coarse grains in the lower part and fine grains in the upper part. The upper part is grayish–green, containing gray mudstone, silty mudstone, siltstone, etc. The bottom section is developed with coarse sandstone, pebbly sandstone, and trough- and plate-shaped oblique bedding [47]. The source supply of section 2 of the Zhiluo Formation is weak, and the sediment grain size is fine. The lower part contains yellow–gray medium

fine arkose and rock debris arkose, and the upper part contains yellow–green, purple–red, and other variegated mudstones, silty mudstones, and siltstone interbedding [48].

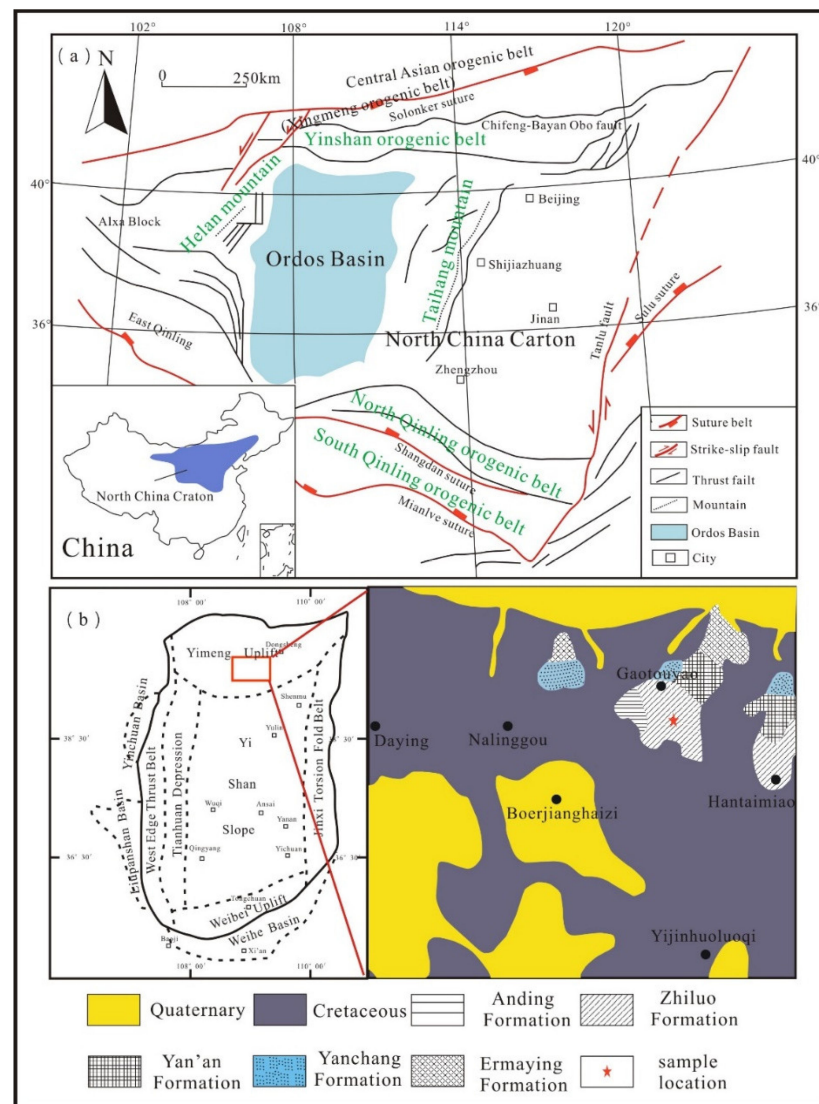


Figure 1. Map of the research area: (a) simplified geological map of north-central China [39]; (b) the division of tectonic units in the Ordos Basin and the regional geological map of the research area.

3. Samples and Methods

In our experiment, we selected a total of thirty-two sandstone samples from the Zhiluo Formation in the research area, including seventeen samples from section 1 and fifteen samples from section 2. This experiment included ordinary thin sections, cast thin sections, physical property analysis, mercury intrusion analysis, and scanning electron microscopy (SEM). The SEM analysis was completed at the Shaanxi Provincial Institute of Geology and Mineral Resources using an FEI MLA650 automatic mineral analyzer. The experimental steps were as follows: mechanical polishing, further polishing of the polished surface using an argon ion polishing instrument, pasting of a conductive film on the surface, sample vacuum pumping (gold spraying at 10–20 nm), and observation under a microscope. The remaining experiments were completed at the Open Research Laboratory of Mineralization and Dynamics of the Ministry of Land and Resources. The cast section was observed at the Open Research Laboratory of Mineralization and Dynamics of the Ministry of Land and Resources of Chang’an University in China with the ZEISS Axio imager D₁m (Zeiss Group, Jena, Germany). The mercury injection experiment was conducted using an AutoPore IV

9510 (Micromeritics, Norcross, GA, USA) fully automatic mercury intrusion instrument, and each sample was processed into a cylinder with a height of 3 cm and a diameter of 2.5 cm. The method and data processing methods refer to GB/T 29171-2012 “Determination of Rock Capillary Pressure Curve”.

4. Results

4.1. Petrology Characteristics

According to Folk’s (1980) sandstone classification method [49], the statistical analysis of the relative content of the samples in the study area revealed that the main rock types of the Zhiluo Formation sandstone are feldspathic sandstone, lithic feldspathic sandstone, and a small amount of feldspathic quartz sandstone (Figure 2). The main detrital components of the sandstone in the study area are quartz, feldspar, and rock debris. The quartz content in the sandstone is the highest, accounting for 38%–48% of the total, with an average content of 42%. It is mostly in a broken and sub-angular shape. Feldspar takes second place, accounting for 21%–27% of the total, with an average content of up to 26%. The difference in rock debris content is significant, ranging from 7% to 13%, with an average content of 9%.

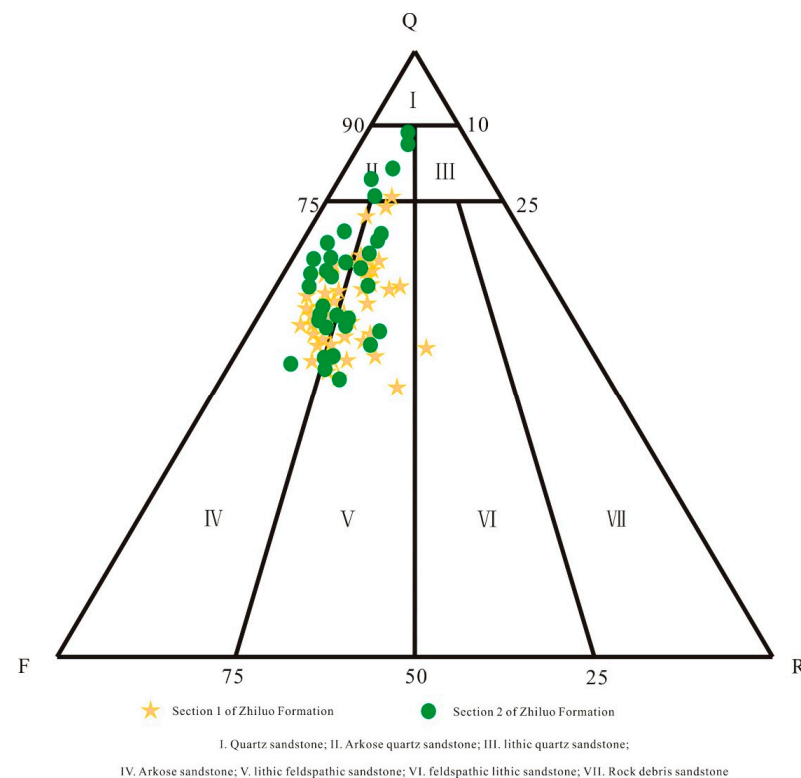


Figure 2. Sandstone type of the Zhiluo Formation. (Q is quartz, F is feldspar, R is rock debris).

4.2. Pore Types and Characteristics

The pores in the study area were divided into two categories: primary and secondary pores. Primary pores correspond to inherent pores formed during initial sedimentation and are influenced by the composition, structure, and sedimentary environment of the rocks. Secondary pores refer to pores that formed after the initial sedimentation of rocks and were reworked by later diagenesis [24]. Primary pores include primary intergranular pores, residual intergranular pores, and interstitial micropores (Figure 3). Secondary pores mainly include dissolution intergranular pores, intraparticle pores, moldic pores, and extra-large pores, as well as intergranular micropores formed by the cementation of authigenic minerals (Figure 4).

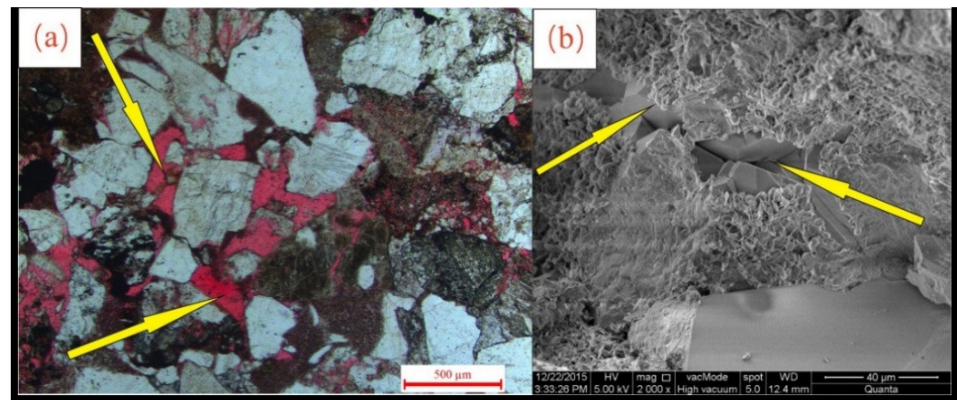


Figure 3. Characteristics of the primary pores in the sandstone of the Zhiluo Formation: (a) residual intergranular pore and (b) intergranular pore.

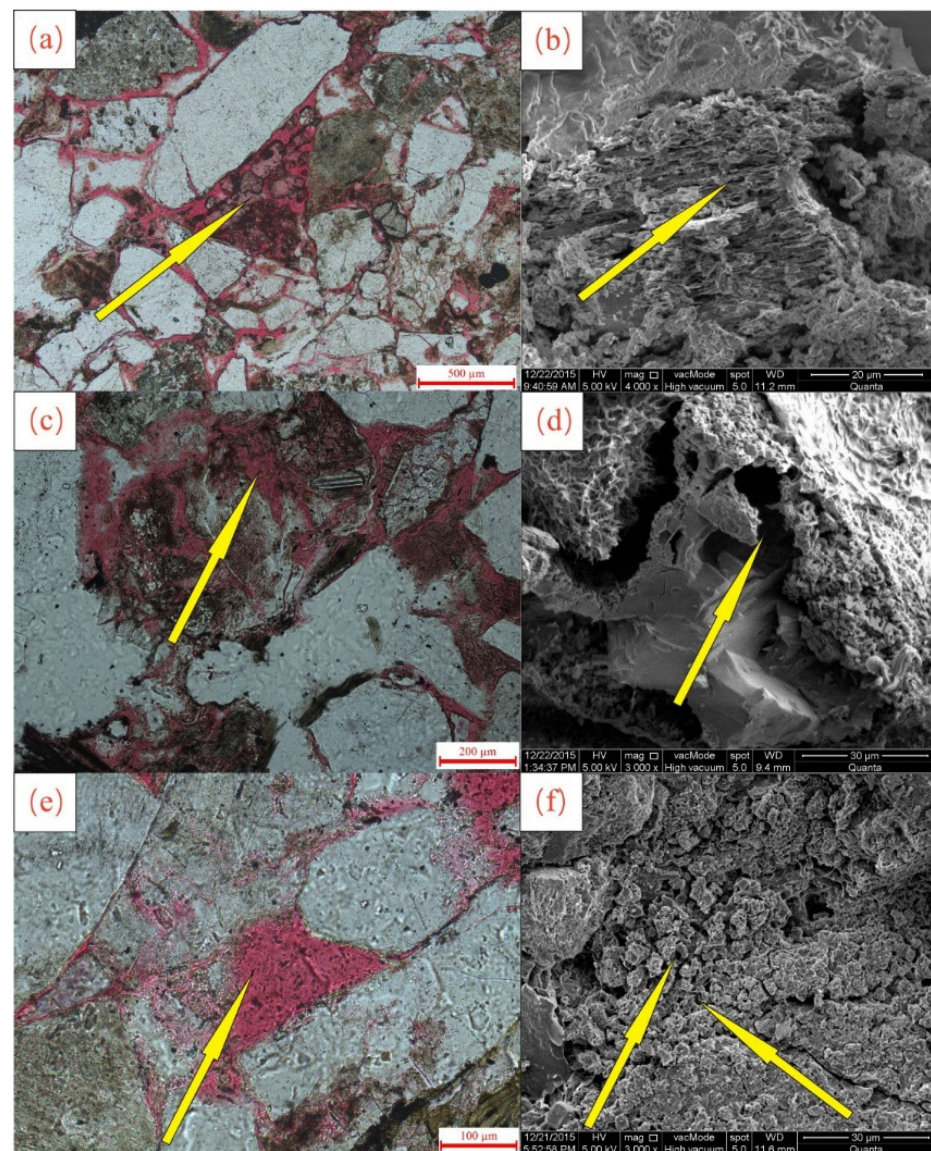


Figure 4. Characteristics of the secondary pores in the sandstone of the Zhiluo Formation: (a) dissolved pores in cement; (b) intragranular dissolved pore in feldspar; (c) intragranular dissolved pore in debris; (d) extra-large pores; (e) moldic pores; and (f) intergranular micropores.

The primary pore characteristics are relatively large pores and throats, good inter-pore connectivity, and the development of pores along the straight edges of particles, with pore diameters of up to 50–80 μm . After the later compaction of the pores, the quartz size increases, and kaolinite, illite, and other clayey cementation processes all produce destructive effects on the primary pores, while the ring-shaped chlorite film formed around the grain edge inhibits, to a certain extent, the secondary enlargement of quartz and feldspar and provides a certain protective effect for the primary pores. The contribution of micropores in the interstitium of the pore structure in the study area is not significant, and the micropores are characterized by a small pore volume and poor connectivity.

The intergranular pores of secondary pores developed mainly as carbonate cementitious dissolution pores; these are spot-like dissolution pores. These dissolution pores are relatively isolated and dispersed, making the formation of a relatively connected pore structure difficult (Figure 4a). Intragranular pores often extend outward along cleavage cracks and fissures and are distributed on the surfaces of particles in a lymphoid manner (Figure 4b). After the partial dissolution of soluble components in rock debris, honeycomb-shaped pores are easily formed; moldic pores are rare and poorly developed, with incomplete dissolution (Figure 4e); and extra-large pores are underdeveloped, with occasional pores equal to or slightly larger than the particle diameter, uneven edges, and residual contours of particles and interstitial materials visible at some boundaries (Figure 4d).

4.3. Throat Types and Characteristics

As throats form channels between pores, the distribution and connectivity of throats affect the reservoir and permeability of pores [6,8,41]. According to the morphological characteristics and genetic classification of the throats, common throats include variable cross-sectional, sheet-like, curved sheet-like, and bundle-shaped throats [50] (Figure 5).

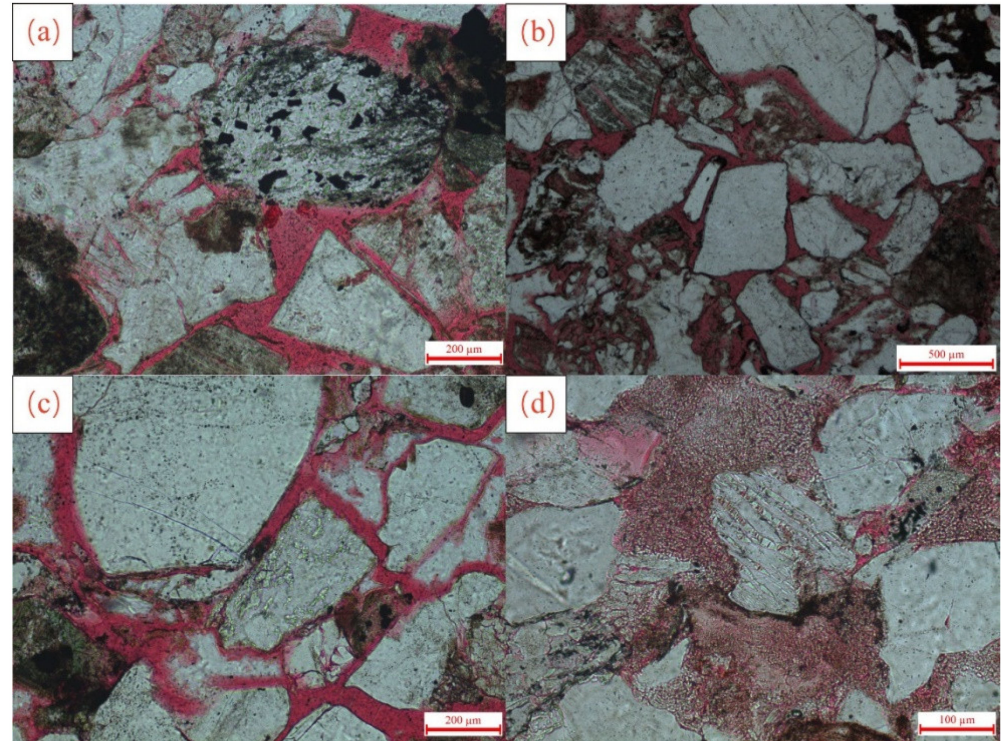


Figure 5. Characteristics of sandstone throats in the Zhiluo Formation: (a) constricted throat; (b) variable cross-sectional throat; (c) sheet-like throat; and (d) bundle-shaped throat.

The variable cross-section throats of the Zhiluo Formation sandstone in the research area mostly exhibit point and line contacts (Figure 5b) with a large throat diameter ratio; this structure is characterized by high porosity and low permeability. Sheet-like throats are rare but are present at the edges of two particles in contact with each other, where the cement has dissolved (Figure 5c). These throats are thin and narrow in shape or curved in shape, corresponding to small, ineffective pores and fine throats characterized by low permeability. The bundle-shaped throats are distributed mostly among the kaolinite cement and are capillary-shaped, with low porosity and permeability (Figure 5d).

4.4. Microcrack Characteristics

Microcracks can effectively connect various pores and improve the pore structure of sandstone [51]. Microcracks are rare in the study area (Figure 6), with an average surface porosity of less than 1%. The microcrack width is approximately 10–40 μm , and microcracks are commonly found in interlayer fractures, brittle mineral compression fractures, and irregular dissolution microcracks along the cleavage direction within feldspar and mica particles. Because mineral cleavage fractures are mostly closed at one end, although they provide a certain porosity improvement effect, their contribution to the permeability is minimal.

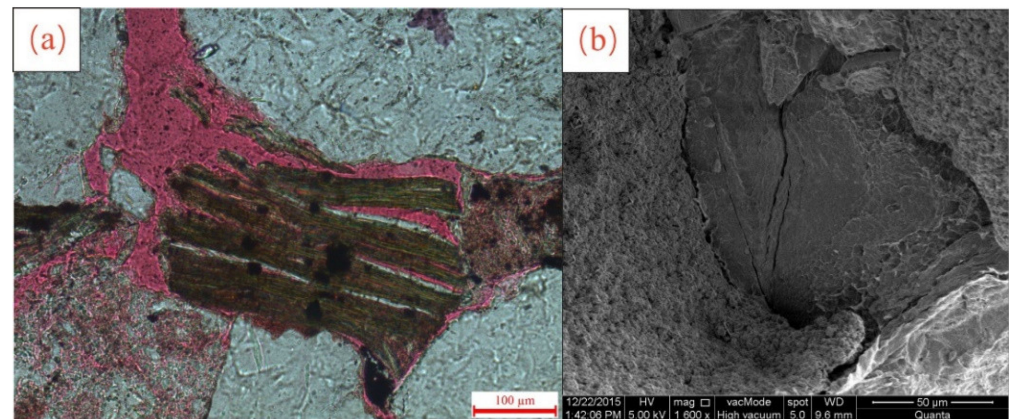


Figure 6. Characteristics of the sandstone microcracks in the Zhiluo Formation: (a) microcracks in mica cleavage and (b) microcracks in mineral fracturing.

4.5. Pore Structure and Fractal Characteristics

Fractality refers to the power exponent relationship between the number of objects and their linear scale, where the fractal dimension is the power exponent [52]. The research object with fractal structures exhibits mutation, discontinuity, and roughness characteristics, and the fractal pore structure does not change with size and is thus a true reflection of the sandstone pore structure [53,54]. Through mercury intrusion experiments, we found that the average mercury-removal efficiency of section 1 of the Zhiluo Formation in the study area is approximately 20%, and the average mercury-removal efficiency of section 2 of the Zhiluo Formation is approximately 29%, indicating that the pore structure characteristics of the first section of the Zhiluo Formation are poor. The pore structure of sandstone in the study area is complex, and the permeability is influenced by the throat characteristics (Figures 7 and 8). The pore concentration and throat distribution are critical in affecting sandstone permeability [41].

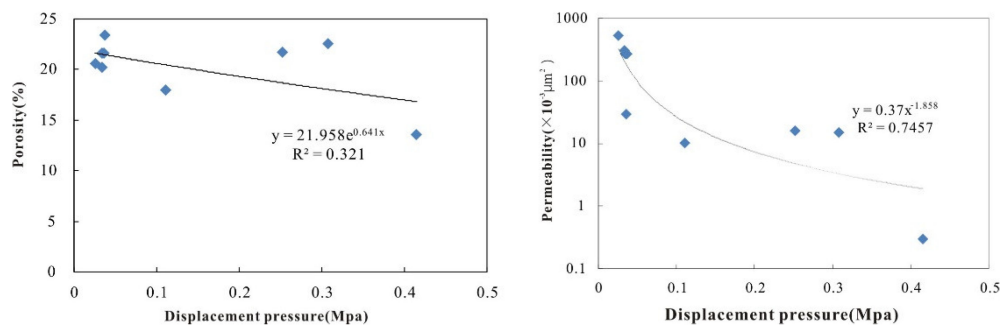


Figure 7. Relationship between the displacement pressure and the physical properties of sandstone in the Zhiluo Formation.

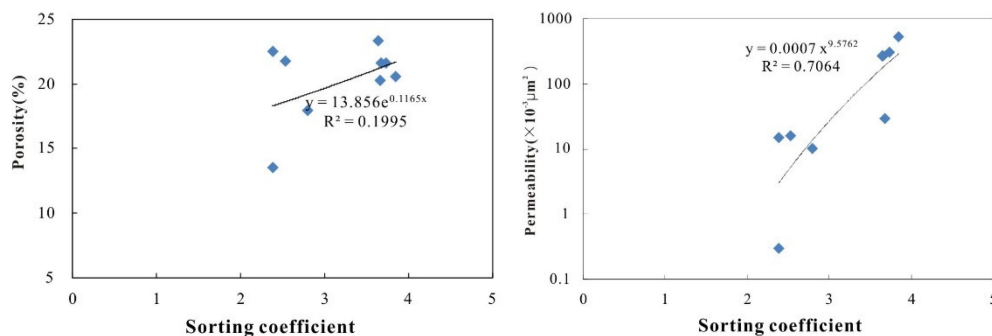


Figure 8. Relationship between the sorting coefficient and the physical properties of sandstone in the Zhiluo Formation.

Through our analysis of the fractal structure characteristics and by fitting the correlation graph between $\lg(S_w)$ and $\lg(P_c)$ in the study area (Figure 9), we found that the linear fitting degree of the Zhiluo Formation sandstone is high and that the sandstone pore structure has good fractal properties. From our observations, as $\lg(P_c)$ increases, the degree of linear correlation increases, indicating that small pore throats have better fractal properties than large pore throats. From the $\lg(P_c)$ - $\lg(S_w)$ diagram (Figures 10 and 11), it can be seen that the sandstone in the study area can be divided into two or three sections. The proportion of small pore throats is relatively high, while the proportions of large and medium pore throats are relatively low. When large pore throats are omitted, two sections can be identified.

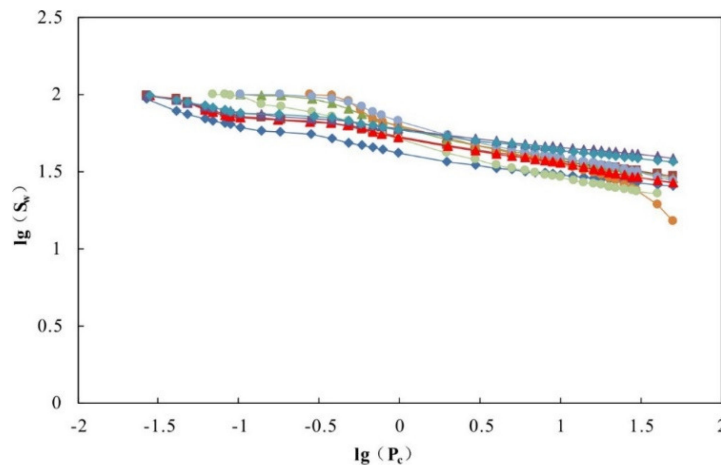


Figure 9. Correlation map of $\lg(P_c)$ - $\lg(S_w)$ in the sandstone of the Zhiluo Formation.

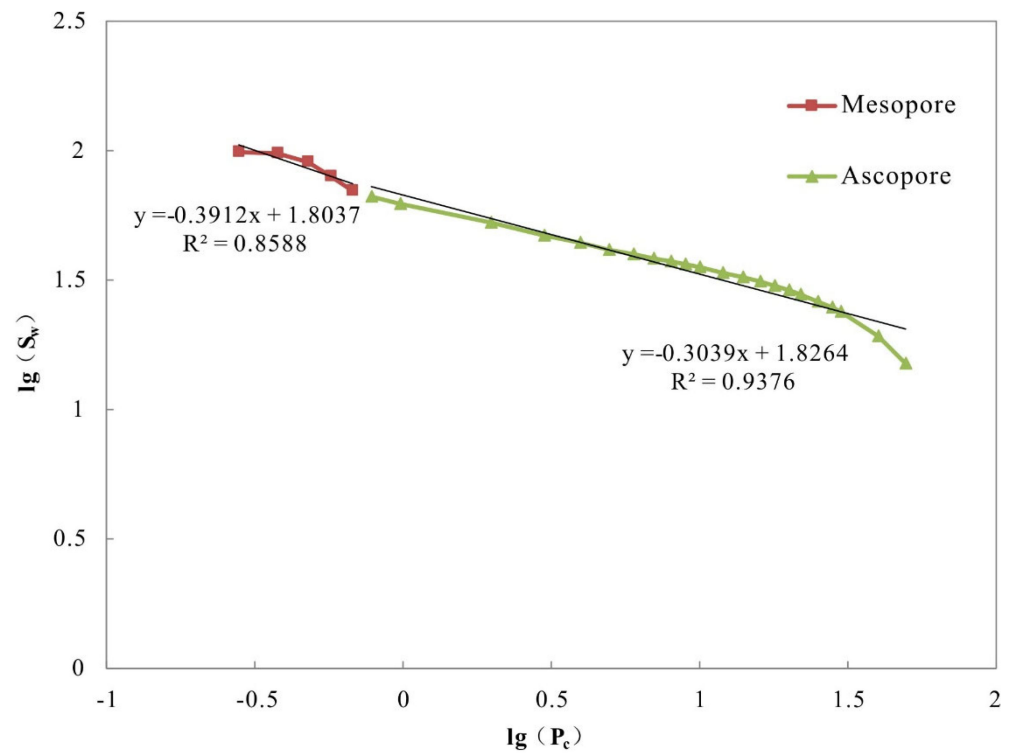


Figure 10. Two-segment $\lg(P_c)$ - $\lg(S_w)$ relationship diagram.

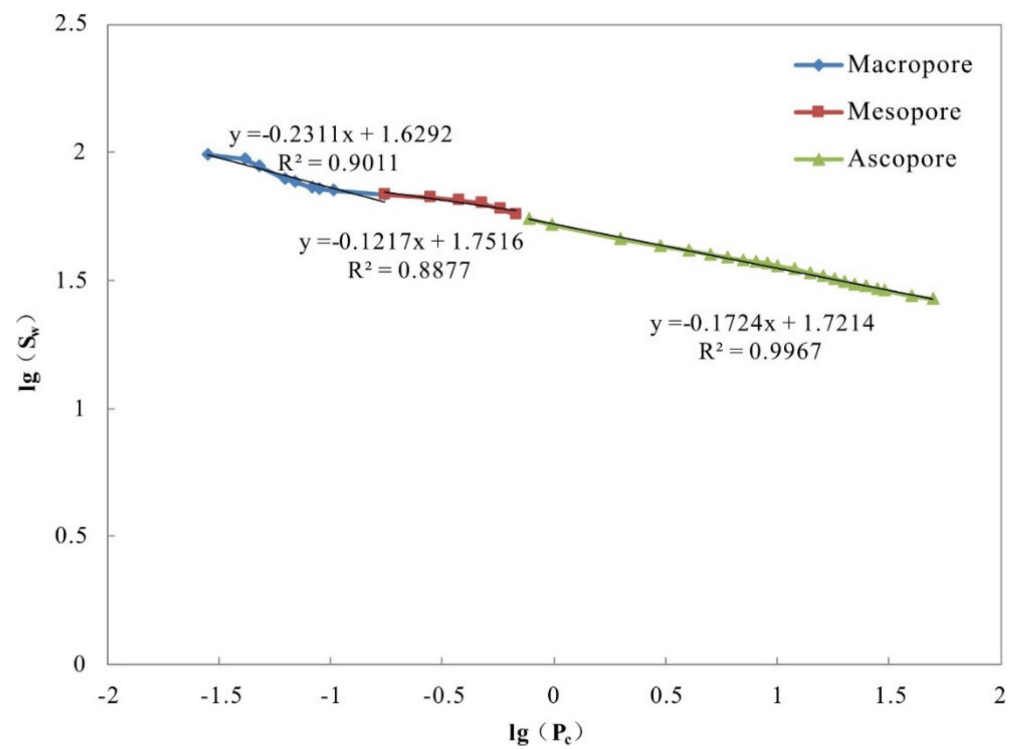


Figure 11. Three-segment $\lg(P_c)$ - $\lg(S_w)$ relationship diagram.

4.6. Pore Structure Types

Differences can be observed in the geometric shape, size, distribution, connectivity, and other throat aspects among different pore throats; these are decisive factors affecting the storage and permeability of permeable sand layers [55]. Parameters such as the porosity, permeability, and displacement pressure of sandstone can be determined through mercury injection experiments. The large number of parameters measured in experiments can allow pore structure characteristics to be analyzed in terms of different aspects. In this study, parameters with good macro- and microcorrelations were selected, and through a comprehensive analysis performed based on multiple aspects, the pore structure of the Zhiluo Formation sandstone in the study area was divided into four types (Table 1, Figures 12–15). The porosity and permeability in Table 1 were obtained from mercury intrusion test data, and the types of pores and throats were identified under a microscope. The pore throat ratio is the ratio of pores to throats obtained through image analysis and mercury intrusion curves. The specific formula is $Bt = Sr / ((S_{max} - Sr))$. Bt is the average pore volume ratio, Sr is the residual mercury saturation, and S_{max} is the maximum mercury saturation.

Table 1. Classification of pore structure of sandstone in the Zhiluo Formation of the research area.

Types	Parameter	Class I	Class II	Class III	Class IV
Macro-characteristics	Permeability ($\times 10^{-3} \mu\text{m}$)	>300	20~300	10~20	<10
	Porosity (%)	>23	20~23	16~20	<16
	Permeability/porosity	>25	1~25	0.1~1	<0.1
Type of pore and throat	Type of pore	Intergranular pores, dissolution pores, and interlayer cracks	Intergranular pores and dissolution pores	Intragranular dissolved pore	Dissolution micropores
	Type of throat	Contracted and variable cross-section	Variable cross-section and sheet-shaped	Sheet-like and curved sheet-like	Curved sheet-shaped and bundle-like
Size of pore and throat	Displacement pressure (Mpa)	<0.03	0.03~0.1	0.1~0.3	>0.3
	Median pressure (Mpa)	<0.5	0.5~1.5	1.5~2.2	>2.2
	Median radius (μm)	>1	0.5~1	0.3~0.5	<0.3
	Face porosity (%)	>21	18~21	15~18	<15
Distribution of pore and throat	Mean value	<9.5	9.5~10.5	10.5~11.5	>11.5
	Skewness	<−0.4	−0.4~−0.1	−0.1~0.1	>0.1
	Sorting coefficient	>3.8	3.1~3.8	2.4~3.1	<2.4
	Coefficient of variation	>0.4	0.3~0.4	0.22~0.3	<0.22
Connectivity degree	Pore–throat ratio	<0.35	0.35~0.36	0.36~0.38	>0.38
Fractal characteristics	Fractal dimension	<2.84	2.84~2.87	2.87~2.9	>2.9

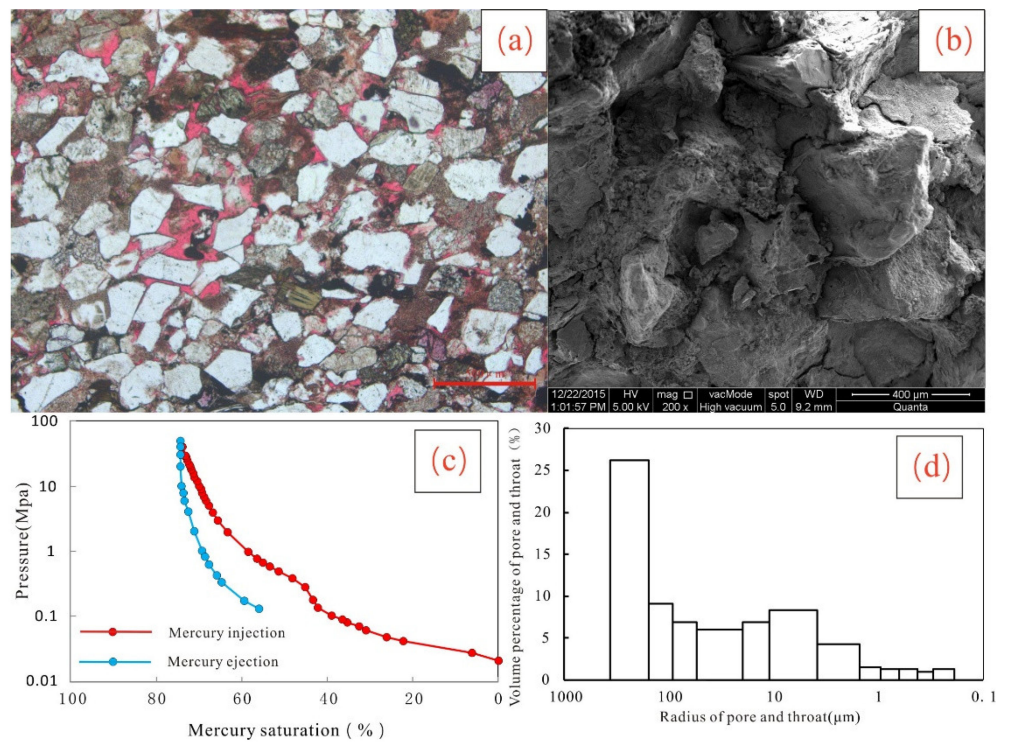


Figure 12. Characteristics of the Class I pore structure: (a) injecting thin sections; (b) SEM; (c) intrusive mercury curve; and (d) pore throat distribution.

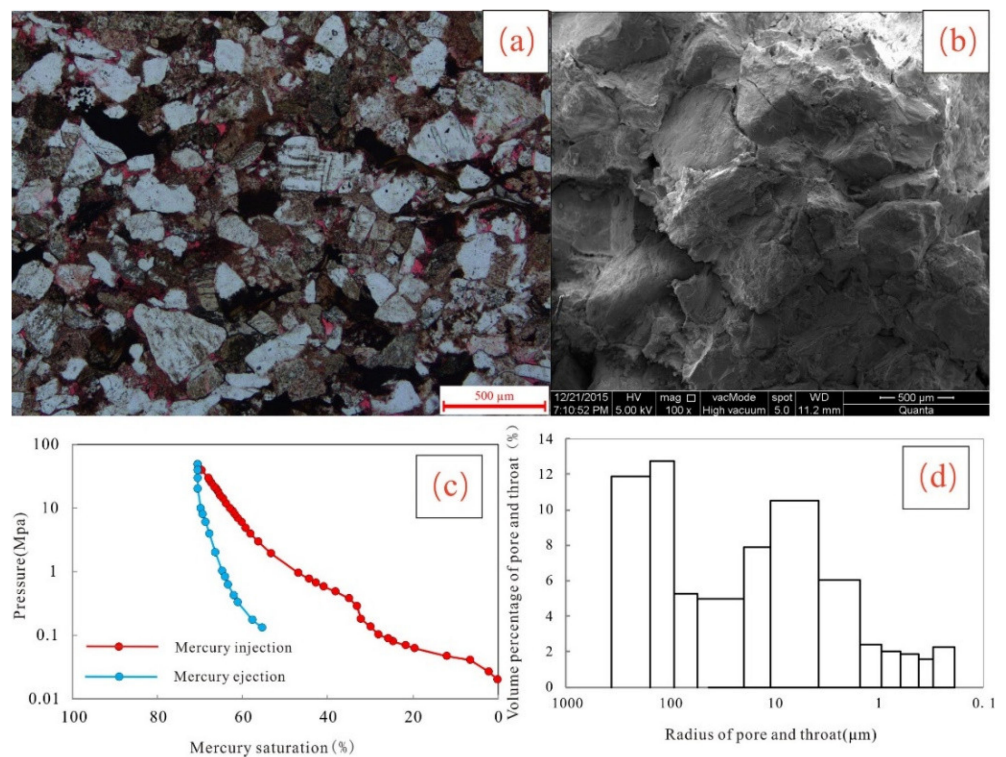


Figure 13. Characteristics of the Class II pore structure: (a) injecting thin sections; (b) SEM; (c) intrusive mercury curve; and (d) pore throat distribution.

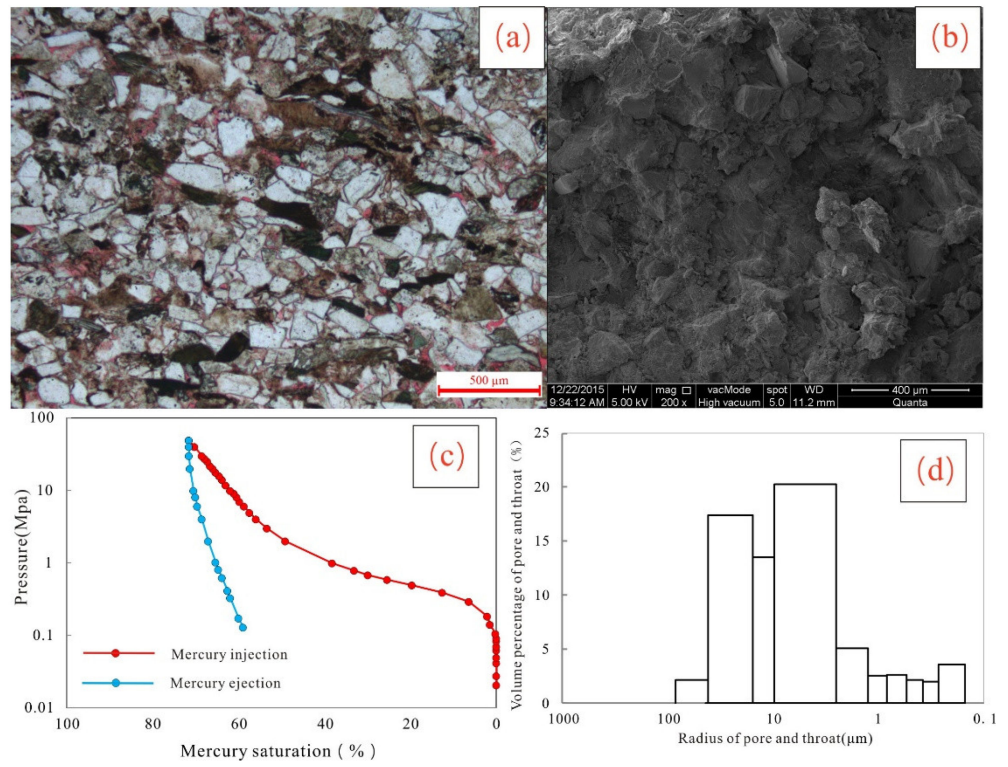


Figure 14. Characteristics of the Class III pore structure: (a) injecting thin sections; (b) SEM; (c) intrusive mercury curve; and (d) pore throat distribution.

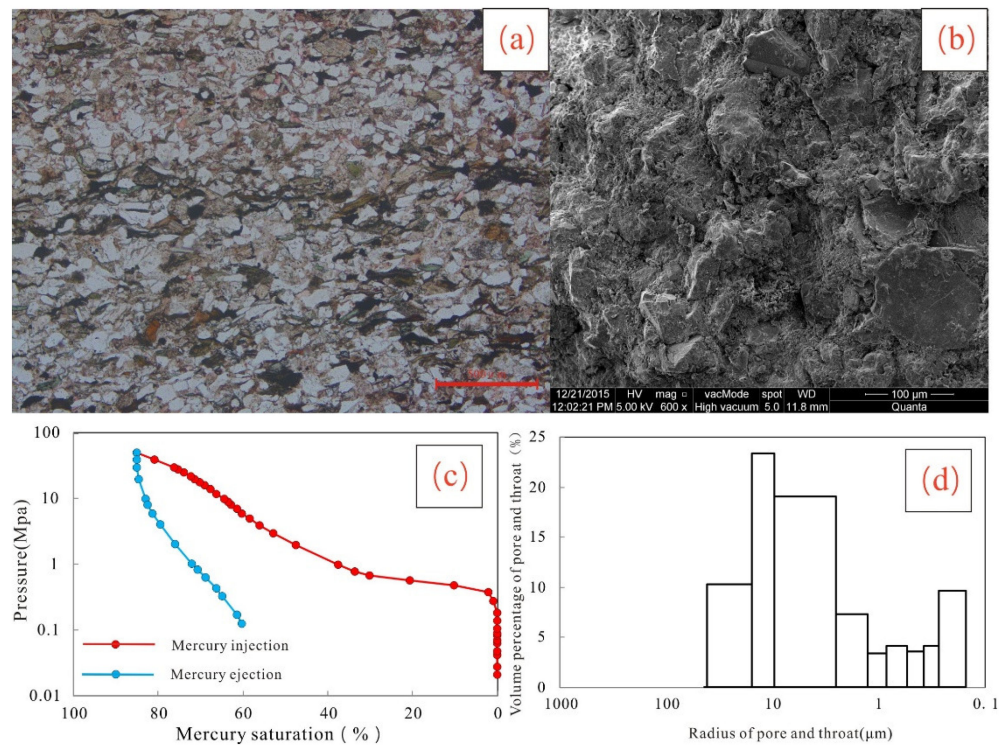


Figure 15. Characteristics of the Class IV pore structure: (a) injecting thin sections; (b) SEM; (c) intrusive mercury curve; and (d) pore throat distribution.

5. Discussion

5.1. Sedimentation and Pore Structure

Sedimentation is the most direct geological factor affecting the pore structure of the sand layer [56,57]. Changes in hydrodynamic forces in different sedimentary environments lead to changes in the accumulation, arrangement direction, and particle size of debris in the sand layer, thus restricting the formation and development of late diagenesis [58,59]. The sedimentary facies of the Jurassic Zhiluo Formation in the study area mainly included braided rivers and meandering rivers [46,60,61]; these facies have laid a good geological foundation for pore development. During the development period of the braided rivers, the hydrodynamic forces were strong, sedimentation was dominated by coarse sandstone, the debris content was high, the particles were angular, the particle size distribution was uneven, the sorting was poor, and the sandstone pores were particularly developed. During the sedimentation period of the meandering rivers, the hydrodynamic forces were weak, and the river channels were relatively stable, but the single-layer sand body was relatively thin and mainly composed of fine sand, and the development of primary pores was poor.

There is an internal relationship between the pore structure and petrology characteristics. The petrological characteristics are the material and spatial framework basis of the pore structure [62,63]. The size of debris particles directly determines the size of the primary pore particles; generally, the larger the debris particles, the larger the intergranular pores. Beard [64] found that the size of debris particles also affects permeability. As shown in Figure 16, the average particle size has certain positive correlations with porosity and permeability. The sandstone in the study area contains mainly arkose and lithic arkose, with low compositional maturity and structural maturity; these rocks are greatly affected by later sedimentation and diagenesis [49]. The quartz content is relatively high and plays a certain compressive role, with a protective and supportive effect on the pore throats. The feldspar debris places second and is mainly related to the secondary dissolution pores formed by the later-stage dissolution of feldspar. In addition, mica and plastic rock debris are subjected to compression, bending, and deformation, with them occupying the primary intergranular pores and even filling them in a pseudo-matrix shape, blocking the intergranular pores and increasing their complexity, thus resulting in a decrease in the relative content of effective pores. Except for debris, the content of interstitial materials in sandstone is relatively high, with a destructive effect on the pore structure. The physical properties of sandstone in the study area deteriorate as the interstitial material content increases (Figure 16), and the permeability changes significantly. This may be due to the development of kaolinite in the sandstone in the study area leading to the blockage of intergranular pores. Although many intergranular pores are present in the kaolinite aggregate and preserve a portion of the porosity, these pores are unable to form effective connectivity, thus greatly reducing the permeability.

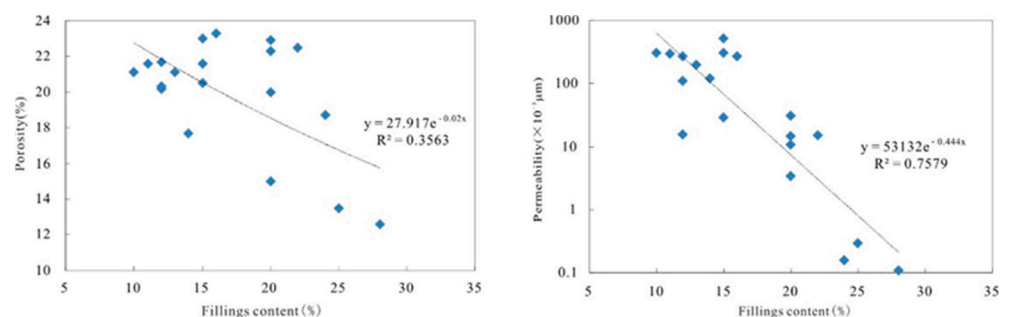


Figure 16. Relationship between the content of sandstone fillers and porosity permeability in the Zhiluo Formation.

5.2. Diagenesis and Pore Structure

Diagenesis plays an important role in controlling the transformation of primary pores and the formation of a variety of secondary pores [65]; compaction and cementation are

the main factors that damage the pore structure of sandstone, while later dissolution plays a certain role in improving the porosity [66]. Pore evolution history studies can reflect the extent to which different diagenetic processes influence pore structures. Due to the synchronous uplift and burial of the Zhiluo Formation with the underlying Yan'an Formation and Yanchang Formation, the period of oil and gas filling is also the same, and the pore evolution patterns of the Yan'an Formation and Yan'chang Formation can be referenced. The evolution of pores can be divided into four stages, namely the early diagenetic stages A and B and intermediate diagenetic stages A and B. Early diagenetic stage A, 165 Ma ago, was shallowly buried, with a paleotemperature of 20–65 °C, belonging to a stage of rapid mechanical compaction and early cementation with immature organic matter. Early diagenetic stage B, 165–138 Ma ago, occurred with an increase in burial depth. The ancient geothermal temperature of 65–85 °C belongs to the cementation stage - the early dissolution stage, with semi-mature organic matter and more obvious cementation of carbonate rocks. Middle diagenetic stage A, 138–120 Ma ago, occurred with a continued increase in burial depth and an ancient geothermal temperature of 85–110 °C. Organic matter entered the peak period of hydrocarbon generation, belonging to the cementation stage - the early dissolution stage. Middle diagenetic stage B, from 120 Ma to the present, is the stage of compaction to late cementation. The burial depth slowly rose to the current depth, with an ancient geothermal temperature of 110–150 °C. The pyrolysis rate of kerogen decreases, organic matter is supersaturated, and the diagenetic environment transitions from acidic to alkaline. Cracks appear, and dissolution weakens until it disappears. However, cementation and compaction make the reservoir denser.

Beard [64] proposed a formula for calculating the original porosity of sandstone: $\varphi_{Raw} = 20.91 + 22.9/So$. The term φ_{Raw} is the original porosity, $So = \sqrt{D_{25}/D_{75}}$, where D_{25} and D_{75} are equivalent to the particle size probabilities of 25% and 75%, respectively. After calculation, the minimum initial porosity of section 1 of the Zhiluo Formation in the research area is 43.81%, the maximum value is 54.26%, and the average value is 48.06%. The initial porosity of section 2 of the Zhiluo Formation is between 43.81% and 53.3%, and the average value is 47.03%. The restoration of residual intergranular pores is mainly used to evaluate the degree of damage caused by compaction on the original intergranular pores [67]. The residual intergranular porosity after compaction can be determined based on the relationships among the cement, residual intergranular pores, dissolution pores, and existing porosity. The residual porosity between particles after compaction is equal to the sum of the total amount of intergranular cement, the total number of dissolution pores, and measured residual intergranular pores; the loss of porosity due to compaction is equal to the initial porosity minus the residual porosity between particles after compaction. As shown in Table 2, through the restoration analysis of the compaction porosity, we found that the original porosity of section 1 of the Zhiluo Formation in the study area was better than that of section 2 of the Zhiluo Formation. Due to the strong compaction effect in the later stage, the relative porosity loss rate of the first section of the Zhiluo Formation is 50.97%, and the relative porosity loss rate of the second section of the Zhiluo Formation is 48.36%. The remaining intergranular porosity of sandstone after compaction, cementation, and replacement equal the porosity of the remaining intergranular pore space in the existing pores [68]. The cementation and replacement loss porosity equals the residual intergranular porosity after compaction minus the residual intergranular porosity after cementation and replacement. The remaining intergranular porosity after replacement is equal to the total amount of intergranular cement plus the total number of dissolution pores. The secondary porosity refers to the portion of the total storage space occupied by dissolution pores [69].

The initial porosity of section 1 of the Zhiluo Formation is 48.06%, and the compaction process resulted in a loss of 24.55%, with a relative loss rate of 50.97%. The early cementation was mainly the cementation of kaolinite, chlorite groups, carbonate, and silica, with a relative porosity loss of 12%, and the later cementation of ferruginous resulted in a porosity loss of 4%. The dissolution after early cementation contributed 3% of the porosity, with a relative contribution rate of 30% to the current porosity. The cracks in the later stage

of cementation only contribute 1% of the porosity, accounting for 6.58% of the current porosity. The initial porosity of section 2 of the Zhiluo Formation is 45.33%, and the compaction process resulted in a loss of 20.97%, with a relative loss rate of 48.36%. The early cementation of clay, carbonate, and siliceous materials resulted in a 10% loss of porosity, while the later cementation of iron-containing materials resulted in a 4% loss of porosity. The dissolution effect after early cementation has constructive significance for the pore structure, contributing 4% of the porosity and 29.9% of the surface porosity. The cracks in the later stage of cementation contribute 1% of the porosity, accounting for 7.52% of the current porosity.

Table 2. Statistical table of porosity loss caused by compaction in the Zhiluo Formation of the study area.

Layer	Initial Porosity (%)	Residual Porosity after Compaction (%)	Compaction Loss Porosity (%)	Relative Loss Rate (%)
section 1 of Zhiluo Formation	$\frac{43.81-54.26}{48.06(13)}$	$\frac{11-35}{24(13)}$	$\frac{13.43-34.64}{24.55(13)}$	$\frac{27.73-75.9}{50.97(13)}$
section 2 of Zhiluo Formation	$\frac{43.81-53.3}{45.33(14)}$	$\frac{14-34}{24(14)}$	$\frac{13.02-33.35}{20.97(14)}$	$\frac{27.69-70.43}{48.36(14)}$

By quantitatively evaluating the loss of primary intergranular pores and the generation of secondary pores in sandstone at different diagenetic stages, a reasonable analysis of the evolution trend of the total porosity of sandstone was conducted, and the corresponding porosity evolution pattern diagram was drawn as follows (Figures 17 and 18). It can be seen from the figure that compaction had the most destructive effect on the pores during late diagenesis in the study area, followed by early cementation, and later cementation had a relatively small impact. In addition, the formation of corrosion and later cracks caused corrosion pores, residual intergranular pores, and cracks to be important components of the current porosity. The relative specific gravity of the effects of compaction and cementation on the pores was evaluated by Housknechet [70]. Assuming that the original sandstone porosity was 40%, it can be seen from Figure 19 that the sandstone of the Zhiluo Formation in the study area is mainly compacted. Some samples from section 1 of the Zhiluo Formation are greatly affected by cementation, and the intergranular porosity of this section is smaller than that of section 2, indicating that the first section has been greatly affected by later diagenesis.

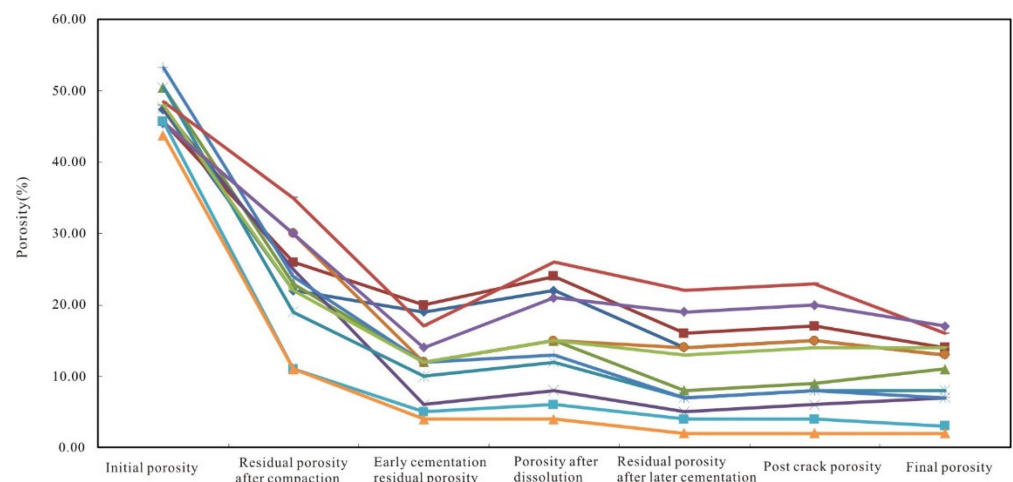


Figure 17. Pore evolution map of section 1 of the Zhiluo Formation.

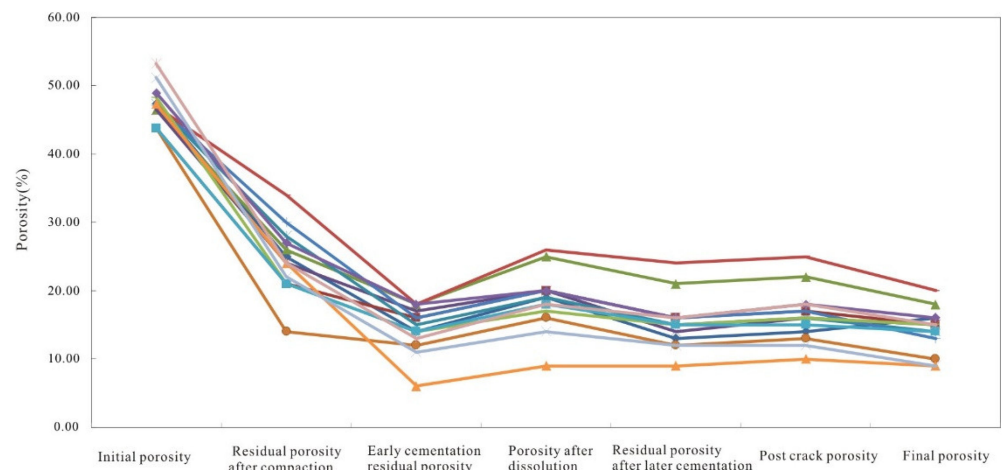


Figure 18. Pore evolution map of section 2 of the Zhiluo Formation.

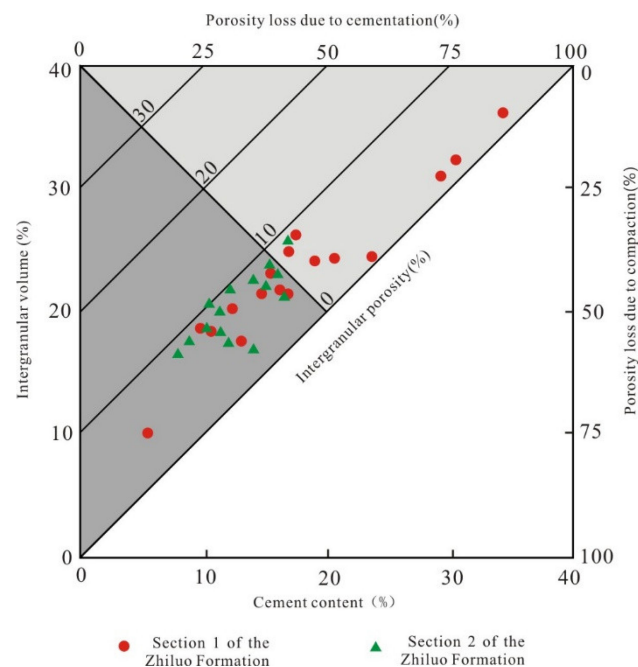


Figure 19. Evaluation of the impact of compaction and cementation on porosity in the study area.

In summary, during the early diagenetic stage of sandstone formation in the study area, compaction caused the directional arrangement, bending deformation, and pseudo heterojunction of plastic particles, resulting in point line contacts and a small amount of concave–convex contacts between particles and causing significant loss of original porosity. The later cementation resulted in porosity losses ranging from 13% to 16%.

5.3. Tectonic Action and Pore Structure

According to previous studies, the overall structure of the Ordos Basin is gentle, with the occurrence of weak tectonic activity during the Zhiluo Formation period [71,72]. Through core observations, we found relatively few high-angle microcracks in the mudstone of the Zhiluo Formation in the study area; in addition, the detachment surface of the mudstone can be observed (Figure 20). Microscopically, microcracks extend far within the layer, with widths of 10 μm –40 μm , and are irregularly distributed. This indicates that a certain degree of tectonic activity has occurred in the study area, and this activity has

played a positive role in improving the pore structure but has had little effect on the overall transformation of the permeable sand layer.



Figure 20. Characteristics of the sandstone core fractures in the Zhiluo Formation: (a) fractures and (b) detachment.

6. Conclusions

1. The primary pores in the study area include primary intergranular pores, residual intergranular pores, and interstitial micropores. The secondary pores mainly include intergranular pores, feldspar dissolution pores, and rock debris dissolution pores. The common throat types include variable cross-sections, sheet-like, curved sheet-like, and bundle-shaped throats.
2. The pore structure of the Zhiluo Formation sandstone in the research area is complex, and its permeability is influenced by the throat characteristics. Based on the pore structure characteristics, we selected characteristic parameters with good correlations and used a combination of macro and micro methods to classify the pore structure types of the Zhiluo Formation sandstone into four types.
3. The main factors affecting the pore structure characteristics of the Zhiluo Formation sandstones in the study area mainly include sedimentation and diagenesis, and the tectonic activity effect is minimal. Compaction and cementation are the main factors that have damaged the pore structure of the sandstone in the study area, and later dissolution has played a certain role in improving the pore structure. Comparatively speaking, section 1 of the Zhiluo Formation has been greatly affected by diagenesis, and section 2 has been greatly affected by sedimentation.

Author Contributions: Methodology, X.L. and X.X.; Software, X.G.; Validation, Z.H. and S.L.; Formal analysis, X.G.; Investigation, Z.H.; Resources, Z.H.; Data curation, X.X. and S.L.; Writing—original draft, X.L.; Writing—review & editing, X.L. All authors have read and agreed to the published version of the manuscript.

Funding: This work was supported by the Shaanxi Provincial Key Laboratory of Land Consolidation, “Soil Pollution Research in Typical Mining Areas in Northern Shaanxi” (2019-ZY01).

Data Availability Statement: The data that support the findings of this study are available from the corresponding author.

Conflicts of Interest: The authors declare no conflict of interest.

References

1. Liao, J.; Xi, A.; Liang, S.; Zhou, X.; Li, Z.; Di, J.; Zhang, W.; Rong, W.; Yu, P. Genetic mechanisms of deep-water massive sandstones in continental lake basins and their significance in micro–nano reservoir storage systems: A case study of the Yanchang formation in the Ordos Basin. *Nanotechnol. Rev.* **2020**, *9*, 489–503. [\[CrossRef\]](#)
2. Yang, H.; Li, Z.; Liu, X. Characteristics and resource prospects of tight oil and shale oil in Ordos Basin. *Acta Pet. Sin.* **2013**, *34*, 1–11.
3. Li, X.; Liu, H.; Pan, S.; Chen, Q.; Rong, W.; Xu, W.; Wang, H.; Huang, J.; Jing, W. Subaqueous sandy mass-transport deposits in lacustrine facies of the Upper Triassic Yanchang Formation, Ordos Basin, Central China. *Mar. Pet. Geol.* **2018**, *98*, 66–77. [\[CrossRef\]](#)
4. Wang, Y. The relationship between oilfield development and pore structure of reservoir rocks. *J. Geosci. Coll. Chengdu* **1982**, *22*, 97–113.

5. Luo, Z.; Wang, Y. Reservoir pore structure, wettability, and oilfield recovery rate. *J. Geosci. Coll. Chengdu* **1980**, *10*, 1–16.
6. Wang, Y.; Zhao, X.; Tang, C.; Zhang, X.; Ma, C.; Yi, X.; Tan, F.; Zhao, D.; Li, J.; Jing, Y. Study on Microscopic Pore Structure Classification for EOR of Low Permeability Conglomerate Reservoirs in Mahu Sag. *Energies* **2023**, *16*, 626. [[CrossRef](#)]
7. Zhang, F.; Jiang, Z.; Sun, W.; Li, Y.; Zhang, X.; Zhu, L.; Wen, M. A multiscale comprehensive study on pore structure of tight sandstone reservoir realized by nuclear magnetic resonance, high pressure mercury injection and constant-rate mercury injection penetration test. *Mar. Pet. Geol.* **2019**, *109*, 208–222. [[CrossRef](#)]
8. Yin, D.; Wang, D.; Zhou, Y.; Zhang, C. Pore Structure Characteristics of Ultra-Low Permeability Reservoirs. *Nat. Resour. Res.* **2021**, *30*, 451–462. [[CrossRef](#)]
9. Mahmud, W.; Yin, X.; Ermila, M. Evaluation of a non-interactive bundle-of-tubes model for calculation of unsteady-state relative permeabilities with laboratory measurements. *J. Porous Media* **2020**, *23*, 1167–1186. [[CrossRef](#)]
10. Rezaee, R.; Saeedi, A.; Clennell, B. Tight gas sands permeability estimation from mercury injection capillary pressure and nuclear magnetic resonance data. *J. Pet. Sci. Eng.* **2012**, *88*, 92–99. [[CrossRef](#)]
11. Zheng, S.; Yao, Y.; Liu, Y. Characterizations of full-scale pore size distribution, porosity and permeability of coals: A novel methodology by nuclear magnetic resonance and fractal analysis theory. *Int. J. Coal Geol.* **2018**, *196*, 148–158. [[CrossRef](#)]
12. Wang, W.; Ye, Y.; Guo, H. Experimental studies of NMR properties of continental sedimentary rocks. *Chin. J. Magn. Reson.* **2001**, *19*, 113–121.
13. Lai, J.; Pang, X.; Li, Y. Typical misinterpretations and scientific concepts in well-logging geologic studies. *Nat. Gas Ind.* **2023**, *10*, 198–211. [[CrossRef](#)]
14. Elliot, T.; Heck, R. A comparison of optical and X-ray CT technique for void analysis in soil thin section. *Geoderma* **2007**, *141*, 60–70. [[CrossRef](#)]
15. Yoshito, N.; Susumu, K. Mathematica programs for the analysis of three dimensional pore connectivity and anisotropic tortuosity of porous rocks using X-ray computed tomography image data. *J. Nucl. Sci. Technol.* **2007**, *44*, 1233–1247.
16. Karayigit, A.; Oskay, R.; Bulut, Y.; Mastalerz, M. Meso- and microporosity characteristics of Miocene lignite and subbituminous coals in the Knk coalfield (Soma Basin, W. Turkey). *Int. J. Coal Geol.* **2020**, *232*, 103624. [[CrossRef](#)]
17. Zou, J.; Fan, C.; Jiang, Y.; Liu, X.; Zhou, W.; Xu, H.; Huang, L. A preliminary study on assessing the Brunauer-Emmett-Teller analysis for disordered carbonaceous materials. *Microporous Mesoporous Mater.* **2021**, *327*, 111411. [[CrossRef](#)]
18. Quiblier, J. A new three-dimensional modeling technique for studying porous media. *J. Colloid Interface Sci.* **1984**, *98*, 84–102. [[CrossRef](#)]
19. Lai, J.; Wang, G.; Fan, Z.; Zhou, Z.; Jing, C.; Wang, S. Fractal analysis of tight shaly sandstones using nuclear magnetic resonance measurements. *AAPG Bull.* **2018**, *102*, 175–193. [[CrossRef](#)]
20. Hazlett, R. Statistical characterization and stochastic 3D modeling of pore networks in relation to fluid flow. *Math. Geol.* **1997**, *29*, 801–822. [[CrossRef](#)]
21. Yao, J.; Zhao, X.; Yi, Y.; Tao, J. The current situation and prospect on digital core technology. *Pet. Geol. Recovery Effic.* **2005**, *12*, 52–54.
22. Zhao, X.; Yao, J.; Tao, J.; Yi, Y. A method of constructing digital core by simulated annealing algorithm. *Appl. Math. A J. Chin. Univ. (Ser. A)* **2007**, *22*, 127–133.
23. Zhu, Y.; Tao, G.; Fang, W.; Xu, X. Lattice Boltzmann Simulation of Permeability in 3D Porous Medium. *Well Logging Technol.* **2008**, *32*, 25–28.
24. Zhu, H. Pore Structure Characterization of Low Permeability Sandstone Reservoir and Application. Ph.D. Thesis, Southwest Petroleum University, Chengdu, China, 2014.
25. Qiao, J.; Zeng, J.; Chen, D.; Cai, J.; Jiang, S.; Xiao, E.; Zhang, Y.; Feng, X.; Feng, S. Permeability estimation of tight sandstone from pore structure characterization. *Mar. Pet. Geol.* **2022**, *135*, 105382. [[CrossRef](#)]
26. Hu, Q.; Ewing, R.P.; Dultz, S. Low pore connectivity in natural rock. *J. Contam. Hydrol.* **2012**, *133*, 76–83. [[CrossRef](#)]
27. Huang, H.; Chen, L.; Sun, W.; Xiong, F.; Ji, W.; Jia, J.; Tang, X.; Zhang, S.; Gao, J.; Luo, N. Pore-throat structure and fractal characteristics of Shihezi Formation tight gas sandstone in the Ordos Basin, China. *Fractals* **2018**, *26*, 1840005. [[CrossRef](#)]
28. Clarkson, C.; Solano, N.; Bustin, R.; Bustin, A.; Chalmers, G.; He, L.; Melnichenko, Y.; Radlinski, A.; Blach, T. Pore structure characterization of North American shale gas reservoirs using USANS/SANS, gas adsorption, and mercury intrusion. *Fuel* **2013**, *103*, 606–616. [[CrossRef](#)]
29. Wang, R.; Sang, S.; Zhu, D.; Liu, S.; Yu, K. Pore characteristics and controlling factors of the Lower Cambrian Hetang Formation shale in Northeast Jiangxi, China. *Energy Explor. Exploit.* **2018**, *36*, 43–65. [[CrossRef](#)]
30. Deng, Y.; Chen, S.; Pu, X.; Yan, J. Characteristics and Controlling Factors of Shale Oil Reservoir Spaces in the Bohai Bay Basin. *Acta Geol. Sin.* **2019**, *94*, 253–268. [[CrossRef](#)]
31. Wang, J.; Han, D.; Deng, Y.; Lin, W.; Su, A.; Wang, C.; Zhang, J.; Zhang, J. Differential Characteristics and the Main Controlling Factors of Shale Oil Sweet Spot Reservoirs in Lucaogou Formation, Jimsar Sag, Junggar Basin. *Geofluids* **2022**, *13*, 6936161. [[CrossRef](#)]
32. Chen, D.; Zhang, Y.; Liu, Y.; Zhong, D.; Meng, H. Characteristics and Controlling Factors of Micro- and Nano-Scale Reservoirs in Continental Shale Sequence of Western Sichuan Depression, China. *J. Nanosci. Nanotechnol.* **2017**, *17*, 6159–6168.

33. Wu, H.; Du, Z.; Ji, Y.; Cao, H.; Meng, L.; Liu, H.; Ma, J. Diagenetic controls on pore structure variations in fan deltaic sandstones of the Eocene Shahejie Formation, Bohai Bay Basin, China: Implications for reservoir quality and oiliness heterogeneities. *Geol. J.* **2023**, *58*, 3191–3219. [[CrossRef](#)]
34. Wang, J.; Jiang, F.; Hu, Q.; Zhang, C.; Yang, X.; Mo, W.; Wang, X.; Qi, Z. A quantitative model and controlling factors of secondary pore development for tight sandstone reservoirs in the carboniferous Benxi Formation, Ordos Basin, China. *Mar. Pet. Geol.* **2023**, *148*, 106034. [[CrossRef](#)]
35. Guo, F.; Peng, X.; Ma, X.; Wang, H. Main controlling factors and oil-bearing potential characteristics of a tight sandstone reservoir: A case study of southwest Ordos Basin. *Energy Explor. Exploit.* **2023**, *41*, 1288–1307. [[CrossRef](#)]
36. Bai, B.; Zhu, R.; Wu, S.; Yang, W.; Gelb, J.; Gu, A.; Zhang, X.; Su, L. Multi-scale method of Nano(Micro)-CT study on microscopic pore structure of tight sandstone of Yanchang Formation, Ordos Basin. *Pet. Explor. Dev.* **2013**, *40*, 354–358. [[CrossRef](#)]
37. Lu, X.; Wang, J.; Ge, L.; Hu, F.; Li, C.; Li, X.; Yu, J.; Xu, H.; Lu, S.; Xue, Q. Pore-scale characterization of tight sandstone in Yanchang Formation Ordos Basin China using micro-CT and SEM imaging from nm- to cm-scale. *Fuel* **2017**, *209*, 254–264. [[CrossRef](#)]
38. Yang, J.; Leng, F.; Yu, H.; Zhao, Y. Micro-pore structure characteristics of the Chang 6 member sandstone reservoir in Huangjiang oilfield Ordos Basin China. *Fresenius Environ. Bull.* **2021**, *30*, 5377–5384.
39. Wu, K.; Cen, D.; Zhang, W.; Yang, H.; Wu, H.; Cheng, X.; Qu, Y.; He, M. Movable Fluid Distribution Characteristics and Microscopic Mechanism of Tight Reservoir in Yanchang Formation, Ordos Basin. *Front. Earth Sci.* **2022**, *10*, 840875. [[CrossRef](#)]
40. Lai, J.; Wang, G.; Cen, M.; Wang, S.; Chai, Y.; Cai, C.; Zhang, Y.; Li, J. Pore structures evaluation of low permeability clastic reservoirs based on petrophysical facies: A case study on Chang 8 reservoir in the Jiyuan region, Ordos Basin. *Pet. Explor. Dev.* **2013**, *40*, 606–614. [[CrossRef](#)]
41. Li, G.; Liu, C.; Zhou, Y.; Wu, H.; Awan, R.; Shi, F.; Wu, Y.; Zang, Q.; Wu, Y. Controlling effects of pore-throat structure and fractal characteristics on the physical properties of ultra-low permeability sandstone reservoirs: A case study of the sixth member of the Yanchang Formation in the Xiaojiahe area, Ordos Basin. *Geol. J.* **2023**, *58*, 1945–1964. [[CrossRef](#)]
42. Ren, D.; Sun, W.; Huang, H.; Nan, J.; Chen, B. Determination of microscopic waterflooding characteristics and influence factors in ultra-low permeability sandstone reservoir. *J. Cent. South Univ.* **2017**, *24*, 2134–2144. [[CrossRef](#)]
43. Liao, J.; Hong, L.; Li, Z.; Tan, K.; Zhao, L.; Yang, J.; Yu, P. Characterization of ultra-low permeability tight sandstone reservoir properties and criteria for hydrocarbon accumulation in Chang 6 member, Huaqing area, Ordos basin. *Front. Earth Sci.* **2022**, *10*, 1013776. [[CrossRef](#)]
44. Zhang, Y.; Chen, Y.; Zhang, Q.; Meng, X. Tectonic sequences of Triassic strata in the southern Ordos Basin, China. *Stratigraphy* **2017**, *13*, 205–219. [[CrossRef](#)]
45. Zhao, J.; Liu, C.; Zhao, J.; Wang, X. Sedimentary facies and its evolution of Jurassic Zhiluo Formation in Ordos Basin. *J. Northwest Univ. (Nat. Sci. Ed.)* **2008**, *38*, 480–486.
46. Cui, L.; Peng, N.; Liu, Y.; Qiao, D.; Liu, Y. Sedimentary Filling Evolution under Paleoclimate Transition—A Case Study from the Middle Jurassic Zhiluo Formation, Ordos Basin. *Minerals* **2023**, *13*, 314. [[CrossRef](#)]
47. Cai, Y.; Han, M.; Zhang, C.; Yi, C.; Li, X.; Zhang, Y.; Wang, G.; Li, H. Geological and Geochemical Characteristics of the Zhiluo Formation in the Bayinqingeli Uranium Deposit, Northern Ordos Basin: Significance for Uranium Mineralization. *Acta Geol. Sin.* **2022**, *95*, 2075–2086. [[CrossRef](#)]
48. Cai, Y.; Ouyang, F.; Luo, X.; Zhang, Z.; Wen, M.; Luo, X.; Tang, R. Geochemical Characteristics and Constraints on Provenance, Tectonic Setting, and Paleoweathering of Middle Jurassic Zhiluo Formation Sandstones in the Northwest Ordos Basin, North-Central China. *Minerals* **2022**, *12*, 603. [[CrossRef](#)]
49. Folk, R. *Petrology of Sedimentary Rocks*; Hemphill Publishing Company: Austin, TX, USA, 1968; p. 184.
50. Lu, S.; Li, J.; Zhang, P.; Xue, H.; Wang, G.; Zhang, J.; Liu, H.; Li, Z. Classification of microscopic pore-throats and the grading evaluation on shale oil reservoirs. *Pet. Explor. Dev.* **2018**, *45*, 452–460. [[CrossRef](#)]
51. Lng, K.; Zhang, Z.; Ring, U.; Faulkner, D.; Gamage, R. Microcracks development and porosity evolution in sandstone, Sichuan basin, China: An experimental approach. *Bull. Eng. Geol. Environ.* **2021**, *80*, 7717–7729. [[CrossRef](#)]
52. Yang, F. *Microscopic Pore Structure Using Fractal Simulation A Case Study of Shengtuo Oilfield*; University of Petroleum: Beijing, China, 2011.
53. Hecht, A. Appolonian packing and fractal shape of grains improving geo mechanical properties in engineering geology. *Pure Appl. Geophys.* **2000**, *157*, 487–504. [[CrossRef](#)]
54. Krohn, C. Sandstone fractal and euclidean pore volume distributions. *J. Geophys. Res.* **1988**, *93*, 3297–3305. [[CrossRef](#)]
55. Amir, M.; Nahla, A. Controls of pore throat radius distribution on permeability. *J. Pet. Sci. Eng.* **2017**, *157*, 941–950.
56. Morad, S.; Al-Ramadan, K.; Ketzer, J.; De Ros, L. The impact of diagenesis on the heterogeneity of sandstone reservoirs: A review of the role of depositional facies and sequence stratigraphy. *AAPG Bull.* **2010**, *94*, 1267–1309. [[CrossRef](#)]
57. Lai, J.; Wang, G.; Wang, Z.; Chen, J.; Pang, X.; Wang, S.; Zhou, Z.; He, Z.; Qin, Z.; Fan, X. A review on pore structure characterization in tight sandstones. *Earth-Sci. Rev.* **2018**, *177*, 436–457. [[CrossRef](#)]
58. Ma, B.; Chen, S.; Yan, W.; Lin, C.; Zhang, H.; Sun, Z.; Zheng, J.; Wang, Y.; Wu, S.; Wang, J. Pore structure evaluation of low permeability clastic reservoirs based on sedimentation diagenesis: A case study of the Chang 8 reservoirs in the Zhenbei region, Ordos Basin. *J. Pet. Sci. Eng.* **2021**, *196*, 107841.
59. Wang, J.; Fu, Y.; Yan, Z.; Fu, J.; Xie, J.; Li, K.; Zhao, Y. Influence of sedimentation and diagenesis on reservoir physical properties: A case study of the Funing Formation, Subei Basin, eastern China. *Earth Sci.* **2021**, *15*, 892–908. [[CrossRef](#)]

60. Wang, Y.; Wu, Y.; Ge, Q.; Pu, Z.; Lu, J.; Zhang, Y.; Xie, X. A Sedimentary Facies-Based Method to Control Water Hazards in the Roof of Deep Jurassic Coals. *Mine Water Environ.* **2023**, *7*, 1. [[CrossRef](#)]
61. Zhao, J.; Liu, C.; Huang, L.; Zhang, D.; Wang, D.; Wang, D. Paleogeography reconstruction of a multi-stage modified intra-cratonic basin—a case study from the Jurassic Ordos Basin, Western North China Craton. *J. Asian Earth Sci.* **2020**, *190*, 104191. [[CrossRef](#)]
62. Zhao, J.; Shen, J.; Qin, Y.; Wang, J.; Zhao, J.; Li, C. Coal Petrology Effect on Nanopore Structure of Lignite: Case Study of No. 5 Coal Seam, Shengli Coalfield, Erlan Basin, China. *Nat. Resour. Res.* **2021**, *30*, 681–695. [[CrossRef](#)]
63. Xi, Z.; Tang, S.; Lash, G.G.; Ye, Y.; Lin, D.; Zhang, B. Depositional controlling factors on pore distribution and structure in the lower Silurian longmaxi shales: Insight from geochemistry and petrology. *Mar. Pet. Geol.* **2021**, *130*, 105114. [[CrossRef](#)]
64. Beard, D.C.; Weyl, P.K. Influence of texture on porosity and permeability of unconsolidated sand. *AAPG Bull.* **1973**, *57*, 349–369.
65. Yin, Y.; Guo, X.; Li, Y. Experimental study on pore structures and diagenesis of the Upper Triassic Yanchang Formation in Ordos Basin China. *Fresenius Environ. Bull.* **2022**, *31*, 6561–6568.
66. Fu, G.; Qin, X.; Miao, Q. Division of diagenesis reservoir facies and its control: Case study of Chang³ reservoir in Yangchang Formation of Fuxian exploration area in northern Shaanxi. *Min. Sci. Technol.* **2009**, *19*, 537–543. [[CrossRef](#)]
67. Cao, X.; Zhong, D.; Liu, J.; Sun, H.; Song, Z.; Cao, T.; Wang, F.; Gong, S. Coupling between Diagenetic Environment and Porosity Evolution—A Quantitative Study of the Zhuhai Formation in the Huizhou Sag, Pearl River Mouth Basin, South China Sea. *Minerals* **2020**, *10*, 170. [[CrossRef](#)]
68. Yang, R.; Wang, F.; Yun, N.; Zeng, H.; Han, Y.; Hu, X.; Diao, N. Pore structure characteristics and permeability stress sensitivity of Jurassic continental shale of Dongyuemiao member of Ziliujing Formation, Fuxing Area, Eastern Sichuan Basin. *Minerals* **2022**, *12*, 1492. [[CrossRef](#)]
69. Zhao, X.; Zhou, W.; Xu, H.; Chen, W.; Jiang, K. Pore evolution characteristics of marine organic-rich shale based on a pyrolysis simulation experiment. *Minerals* **2022**, *12*, 1098. [[CrossRef](#)]
70. Houseknecht, D.W.; Hathon, L.A. Relationships among thermal maturity, sandstone diagenesis, and reservoir quality in Pennsylvanian strata of the Arkoma basin. *AAPG Bull.* **1987**, *71*, 568–569.
71. Sun, Y.; Jiao, Y.; Wu, L.; Rong, H. Relations of Uranium Enrichment and Metal Sulfides within the Shuanglong Uranium Deposit, Southern Ordos Basin. *J. Earth Sci.* **2022**, *33*, 395–408. [[CrossRef](#)]
72. Liu, C.; Zhao, H.; Gui, X.; Que, P.; Zhao, J.; Wang, J. Space-Time coordinate of the evolution and reformation and mineralization response in Ordos Basin. *Acta Geol. Sin.* **2006**, *80*, 617–638.

Disclaimer/Publisher’s Note: The statements, opinions and data contained in all publications are solely those of the individual author(s) and contributor(s) and not of MDPI and/or the editor(s). MDPI and/or the editor(s) disclaim responsibility for any injury to people or property resulting from any ideas, methods, instructions or products referred to in the content.